

X-ray selected AGNs: The Clustering Properties

E. Ghaffarsedeh¹, J. Quenby¹

¹*Astrophysics Group, Blackett Laboratory, Imperial College, Prince Consort Rd, London SW7 2BZ, UK*

23 August 2019

ABSTRACT

Clustering properties of two samples of X-ray selected AGNs are compared with IR/Optical galactic samples. These are the Einstein Observatory Extended Medium Sensitivity Survey: EMSS (Maccacaro et al. 1991), with flux limit of $> 3.25(10^{-14})$ erg cm⁻² sec⁻¹ (0.5–2.0 keV), redshifts up to 2.83 and a sky coverage of 778 deg²; and an all sky sample of 654 ROSAT detected radio quasars (Brinkmann et al. 1997), with a uniform flux limit of a few (10^{-13}) erg cm⁻² sec⁻¹ (0.1–2.4 keV) and redshifts up to 3.886. The cosmological dipole moment is calculated for these samples, yielding the values of $b\Omega_o^{-0.6}$ (where b is the bias parameter, and Ω_o is the present value of the cosmological density parameter). We find this factor to be 0.68 ± 0.22 for the EMSS sample, and 1.02 ± 0.014 for the quasars sample. Comparing these values with that of the IRAS 1.2 Jy sample (1.95 ± 0.096), suggests that these AGNs are less clustered than the IRAS galaxies. For each sample there is a depth at which the amplitude of the dipole growth curve saturates. This convergence radius (R_{conv}) is found to be $\sim 300 - 400 h^{-1}$ Mpc for the EMSS sample and $\sim 450 - 500 h^{-1}$ Mpc for the ROSAT detected quasars sample, which suggests that X-ray AGNs have a much deeper contribution to the Local Group (LG) motion compared to the galaxy and cluster samples. Also the maximum amplitudes at saturation are found to be 405 ± 103 km/sec for the EMSS AGNs and 617 ± 8 km/sec for the quasar sample, which suggests that the lower the flux limit of the sample (ie. the more sensitive the sample), the lower the maximum amplitude at the region of saturation, therefore the less clustered the sample. Using the properties of the angular and spatial correlation functions for these samples, we find: $b_{IRAS}/b_{quasars} = 3.61 \pm 2.7$; $b_{IRAS}/b_{EMSS} = 8.46 \pm 6.4$ and $b_{quasars}/b_{EMSS} = 2.35 \pm 0.2$. Using Chi-squared minimisation, we have fitted the angular correlation functions using the standard power law model of the form: $W(\theta) = A\theta^{-\delta}$, and the spatial correlation functions using the power law model of the form: $\xi(r) = (r/r_0)^{-\gamma}$. For the angular correlation functions, we find $A \sim 0.6$ for the AGN auto-correlations and $A \sim 0.2 - 0.3$ for the AGN-IRAS galaxy cross-correlations. Also δ is found to be $0.8 - 1.1$. In the spatial correlation analysis, we find $r_o \sim 3.5 - 5.1 h^{-1} Mpc$ and $\gamma \sim 1.4 - 1.7$. The bias factor resulting from the IR/Optical galaxies may not be the true representative of this parameter, due to the local nature of those samples, whereas AGN samples are deep/far enough to give a more accurate value of this parameter.

Key words: AGNs – Clustering – Large scale structure of the universe – Cosmology: Observations

1 INTRODUCTION

A way of investigating the large scale clustering properties of extragalactic objects, is to analyse their cosmological dipole moment. The anisotropy of the Cosmic Microwave Background (CMB) radiation and the solar motion relative to the Local Group of galaxies (LG) implies that the LG has a peculiar velocity of ~ 600 km/sec towards $(l, b) = (277^\circ, 30^\circ)$ (cf. Rowan-Robinson, Lynden-Bell, 1988). According to the

linear perturbation theory (Peebles, 1980), the peculiar motion of the LG is in the same direction as the gravitational acceleration arising from the distribution of mass outside of the LG. Attempts to trace this mass distribution responsible for the gravitational acceleration associated with the peculiar velocity of the LG have been made using the IRAS galaxies (Yahil, Walker & Rowan-Robinson, 1986; etc.), Optical galaxies (Lahav, 1987; etc.), X-ray clusters (Lahav et al., 1989) and X-ray AGNs (Miyaji & Bolt, 1990).

The spatial extend of the distribution of mass inhomogeneities that cause the LG motion has been a matter of debate. The most probable cause for this motion as well as for the observed peculiar motions of other galaxies and clusters is gravitational instability. This is supported by the fact that the gravitational dipole (acceleration) of many different samples of extragalactic mass tracers is well aligned with the general direction of the CMB dipole (Rowan-Robinson et al., 1990; Strauss et al. 1992; etc.).

However what still seems to be under discussion is the depth from which density fluctuations contribute to the gravitational field that shapes the LG motion. The largest such depth, is defined by the dipole convergence depth, R_{conv} , which is that depth where the true gravitational acceleration converges to its final value. The apparent value of R_{conv} differs from sample to sample, normally in the range 40 to 100 h^{-1} Mpc (for galaxy samples), with a strong dependence on the sample's characteristic depth. Cluster samples, such as Optical *Abell/ACO* cluster sample is volume limited out to large enough depth ($\sim 240h^{-1}$ Mpc) to allow a more reliable determination of R_{conv} which was found to be $\sim 160h^{-1}$ Mpc (Scaramella et al., 1991; Plionis & Valdernini, 1991; Branchini & Plionis, 1996). Therefore studies using clusters of galaxies as a probe, suggests that a significant part of the LG's motion is caused by structures at much greater distances than 100 h^{-1} Mpc. Recently, this result has been supported using X-ray cluster samples, which are free of the various systematic effects from which the optical catalogues suffer (Plionis & Kolokotronis, 1998).

In the following sections, we will be discussing the dipole moment for the EMSS AGNs and the ROSAT detected quasars sample, from which we will find the values of the bias parameters. Furthermore, to investigate the clustering of objects at small scales, we study their angular and spatial correlation properties.

One of the most common statistical characterizations of the clustering properties of galaxies and other extragalactic objects is the three-dimensional two point correlation function (Peebles, 1980), $\xi(r)$, in which one uses information on redshift, longitude and latitude for each object. Note that this is the Fourier transform of the power spectrum of the galaxy distribution (Peacock & Nicholson, 1991), where the power spectrum is the square of the absolute value of the Fourier transform of the density field of galaxies. An easier way to investigate these clustering properties, however, is the two-dimensional two point angular correlation function, $w(\theta)$, in which we only need information on the longitude and latitude for each object.

Later on, we will be discussing the results of the auto and cross-correlation functions between various samples, from which we can deduce the values of the relative bias parameters.

2 DESCRIPTION OF DATA

The EMSS is a statistically complete (96%) and well-defined sample of 835 serendipitous X-ray sources (of which more than 400, are AGNs) detected in IPC images of the high Galactic latitude sky obtained with the IPC on board the Einstein Observatory. It has limiting sensitivities from $5(10^{-14})$ to $3(10^{-12})$ erg cm^{-2} sec^{-1} in the 0.3-3.5 keV en-

ergy band (typically $> 3.25 (10^{-14})$ erg cm^{-2} sec^{-1} in the 0.5-2.0 keV energy band), redshifts up to 2.83 and a sky coverage of 778 deg^2 (for further details, see Stocke et al., 1991; Gioia et al., 1990; Maccacaro et al., 1991).

The sample of 654 ROSAT detected radio quasars (Brinkmann et al., 1997), is an all sky survey with a uniform flux limit of a few (10^{-13}) erg cm^{-2} sec^{-1} (0.1-2.4 keV) and redshifts up to 3.886. This sample has been compiled from the Veron-Cetty-Veron catalogue detected by ROSAT in the ROSAT All-sky survey (Voges, 1992), as targets of pointed observations, or as serendipitous sources from pointed observations as available publicly from the ROSAT point source catalogue (ROSAT-SRC, Voges et al., 1995)

3 A BRIEF REVIEW OF THE TESTS FOR COSMOLOGICAL EVOLUTION FOR XRAY SELECTED AGNS

To test the evolution in cosmological objects, one normally investigates the logN-logS relation, the $\langle V_e/V_a \rangle$ test and the differential luminosity function.

The logN-logS relation for the EMSS AGNs and the 654 ROSAT detected quasars are shown in Figure 1. It appears that these AGNs have gone through a positive luminosity evolution with time, ie. they have either been more luminous or more common / numerous in the past. Also note that the flux at which the logN-logS curve stops increasing is an approximation for the flux limit of the sample. Errors have been estimated as pure Poissonian. Furthermore, using the maximum likelihood method, each curve has been fitted with a power law model. As can be seen, a steeper slope is found for the EMSS sample (-1.57 ± 0.1) compared to the 654 quasar sample (-1.13 ± 0.36), from which it might appear that the EMSS AGNs have evolved more in time. However, considering the 1σ errors, the slopes are consistent with -1.5 which is the value found for non-evolving objects.

Next, the differential X-ray Luminosity Function (XLF) for both the EMSS sample and the 654 quasar sample, are presented in Figure 2 and Figure 3. To obtain these, we have used the method of summing inverse accessed volumes, as described in Schmidt (1968); Maccacaro (1991) and Page et al. (1996). Therefore, the XLF is calculated as:

$$\Phi(L, z) = \frac{dN(L)}{dL} = \sum_1^N \frac{1}{V_s \cdot dL} \quad (1)$$

where, V_s is the volume in the universe searched to find a particular object, and dL corresponds to the luminosity bins. Also the error bars are calculated using:

$$\left(\sum_1^N \frac{1}{V_s^2} \right)^{1/2} \quad (2)$$

Assuming only the luminosity evolution model (since this is more commonly accepted), a single power law model has been fitted to each individual XLF corresponding to different redshift shells and a different slope has been found for each, as shown on the plots.

Note that it is more common to fit a LF with two power laws, but in this calculations, a single power law gave a reasonably good fit (The goodness of the fits can be tested using the 2D K-S test). Finding different slopes for each redshift

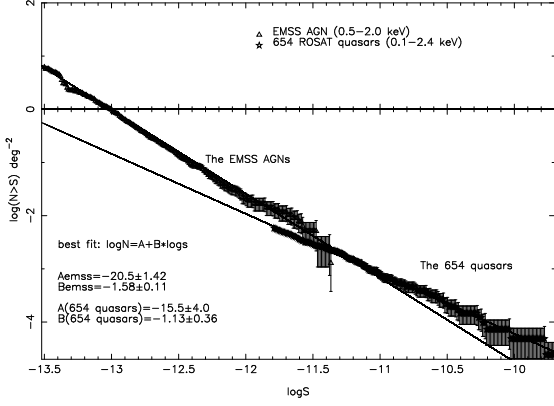


Figure 1. The differential logN-logS relation for the EMSS and the 654 ROSAT detected AGNs

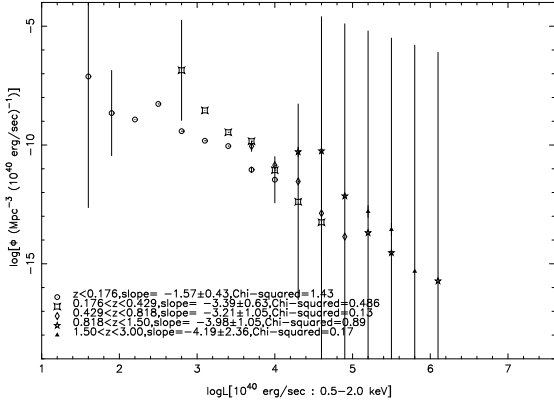


Figure 2. The differential XLF for the EMSS AGNs

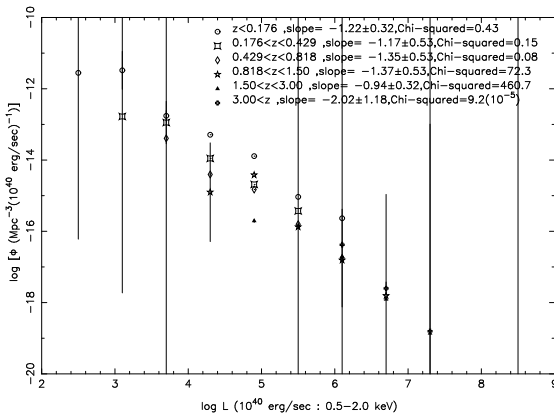


Figure 3. The differential XLF for the 654 ROSAT detected quasars

shell, suggests that these AGNs have evolved differently at different periods of time.

The XLF is used to calculate the selection function, which is used in dipole and correlation function analysis. In dipole analysis, the weight corresponding to each object is proportional to the inverse of the selection function. Also in the analysis of the spatial correlation function, the random sample is selected so as to have the same selection function (i.e. the same redshift distribution) as the original sample. In most common cases of flux limited extragalactic object catalogues, one has to take into account the effects of the consequent undersampling of the density field especially at large distances, where the radial selection functions rapidly decline. Assuming that the unobserved galaxies are spatially correlated with those included in catalogue, the usual procedure to correct for the missing population is to weight each observed object at a distance r by a factor $\propto \frac{1}{\Phi(r)}$, which is the reciprocal of the portion of the LF that can not be sampled at that distance due to the flux limit of the catalogue. Therefore, the weight becomes:

$$w_i = \phi^{-1}(r_i) r_i^{-2} \quad (3)$$

where:

$$\phi(r) = \frac{1}{n} \int_{L_{min}(r)}^{L_{max}} \Phi(L) dL \quad (4)$$

is the selection function.

$\Phi(L)$ is the luminosity function, $L_{min}(r) = 4\pi r^2 S_{lim}$ is the minimum luminosity that an extragalactic object can have in order to be visible at a distance r which is determined by the flux limit of the sample. L_{max} is the maximum luminosity of such an object.

Note that the average density, n , is calculated as:

$$n = \int_{L_{min}}^{L_{max}} \Phi(L) dL \quad (5)$$

where L_{min} is the minimum luminosity of the object.

Note that the selection function is inversely proportional to r , and this acts as a compensating effect for the fact that poor sampling occurs at large redshifts.

4 THE COSMOLOGICAL DIPOLE MOMENT

In this section, we give a summary on how to calculate the amplitude of the dipole growth curve as a function of the radial distance. Basically, the dipole moment is defined as:

$$D = \sum_{i=1}^{i=N} w_i r_i \quad (6)$$

where r_i is the unit vector pointing at the position of each object and N is the total number of such objects within the distance considered. The weight (w_i) is calculated as shown in equation 3.

Using the linear perturbation theory, and the above definition of the dipole, the relation between the observed peculiar velocity of an observer, V_p , and that predicted by its gravitational acceleration, g , as long as the two vectors are well aligned is:

$$V_p(r) = \frac{H_0 \beta}{4\pi n} \sum_{i=1}^{i=N} \frac{\phi^{-1}(r_i) r_i}{|r_i|^3} = \beta g(r) \quad (7)$$

where: $\beta = \frac{\Omega_o^{0.6}}{b}$, (b is the bias parameter).

Note that $V_p(r)$ decreases with increasing r , therefore the more distant objects have less contribution to the acceleration of the LG, but do continue to add to the peculiar velocity.

From the above equation, the three components of the acceleration generated by each object on the LG can be calculated (V_x, V_y, V_z). The force can then be smoothed out to guarantee linearity, where the function Smooth is defined as:

$$Smooth(r^2, r_{min}) = \frac{1}{\max(r^2, r, r_{min}^3)} \quad (8)$$

ie. each component is multiplied by the function smooth.

We then sum over shells to build up the three cartesian components of the cumulative dipole (acceleration) at radius r . Finally we calculate the amplitude of the cumulative dipole at the same radius, using:

$$V_{cum} = \sqrt{V_{cum-x}^2 + V_{cum-y}^2 + V_{cum-z}^2} \quad (9)$$

where V_{cum-x} , V_{cum-y} , V_{cum-z} are the three components of the cumulative acceleration.

Note that the moments of the objects are affected by the discreteness effects or the shot noise errors, which increase with redshift because of the rapidly declining selection function. These effects introduce a variance in the dipole amplitude and direction. To calculate these effects, we can use the method of Strauss et al. (1992), Hudson (1993) and Branchini & Plionis (1996), as follows:

$$\sigma_z^2 = \sum_{i=1}^{i=N} w_i^2 (z_i / |r_i|^3)^2 \quad (10)$$

Therefore:

$$\sigma_{3D} = \sqrt{\sigma_x^2 + \sigma_y^2 + \sigma_z^2} \quad (11)$$

and the corresponding error along the line of sight (1D error) is:

$$\sigma_{1D} = \frac{\sigma_{3D}}{3^{1/2}} \quad (12)$$

5 THE RESULTS OF THE DIPOLE MOMENT ANALYSIS

The resulting dipole growth curves for the EMSS sample is shown in figure 4.

As can be seen, there is no signal observed at small depths (ie. $< 40h^{-1}Mpc$), indicating insignificant contribution to the LG motion from the nearby objects. This is expected, since there are not many objects in the EMSS sample with distances $< 40h^{-1}Mpc$. The amplitude of the dipole growth curve saturates at rather large depths of $> 300h^{-1}Mpc$. However from distances of about $300h^{-1}Mpc$, the amplitude of the dipole increases only by small amounts. Therefore $R_{conv} \sim 300 - 400h^{-1}Mpc$, which is the depth from which these AGNs contribute to the acceleration of the LG via their gravitational attraction. Note that there are relatively large error bars, particularly at larger depths, which put limits to the accuracy of the value of R_{conv} .

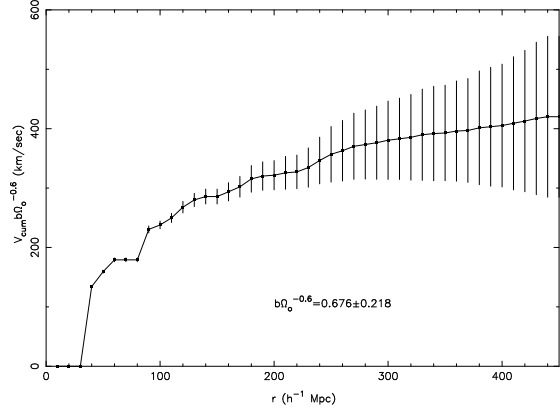


Figure 4. The Dipole Growth Curve for the EMSS AGNs

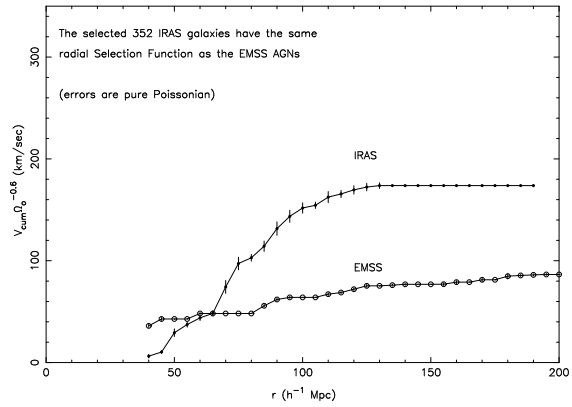


Figure 5. Comparing the Dipole Growth curves for the EMSS AGNs and the IRAS galaxies

From this analysis, the value of $b_{EMSS}\Omega_o^{-0.6}$ is found to be 0.68 ± 0.22 . This depends on the present value of the cosmological density parameter (cf. $\Omega_o = 1$ for the Einstein-de Sitter universe). For IRAS galaxies, $R_{conv} \sim 40 - 100h^{-1}Mpc$, therefore comparing this with the one for the EMSS sample, suggests a dependence between the maximum effective depth of the sample and the convergence radius, ie. the deeper the sample (in distances), the larger the value of R_{conv} .

To further compare the dipole moments of the EMSS AGNs with that of the IRAS 1.2 Jy galaxies, we have selected a sample of 352 IRAS galaxies with the same selection function as the EMSS sample (ie. the same redshift distribution) and plotted the cumulative dipole growth curves for both samples, as shown in figure 5.

In these analysis, we have plotted both curves with bias parameter of 1.0. As can be seen at almost all distances, the dipole moment of IRAS galaxies dominates that of the EMSS. It appears that IRAS galaxies have stronger contributions to the motion of the LG than the EMSS AGNs. In other words, IRAS galaxies are more clustered than the EMSS AGNs at scales of $< 200h^{-1}Mpc$ (this is compared to the underlying mass distribution), which is consistent with the values of the bias parameter (assuming the Einstein-de Sitter universe).

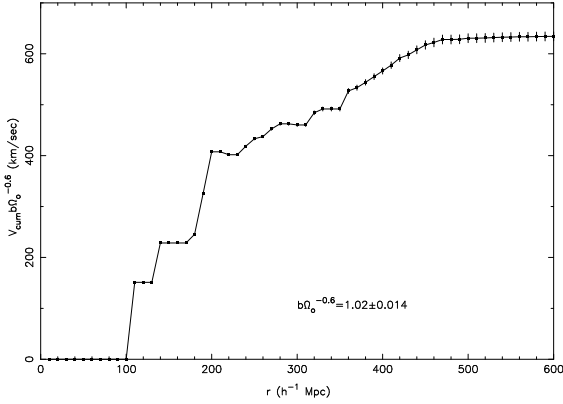


Figure 6. The Dipole Growth Curve for the 654 ROSAT detected radio quasars

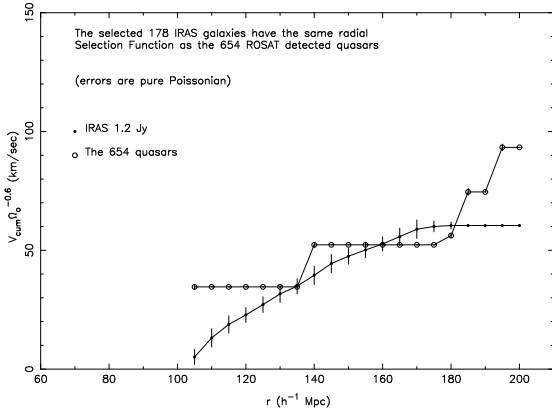


Figure 7. Comparing the Dipole Growth curves for the 654 ROSAT detected quasars and the IRAS galaxies

Similarly, the dipole growth curve for the 654 ROSAT detected radio quasars, is shown in Figure 6.

For this sample, $R_{conv} \sim 450 - 500 h^{-1} \text{Mpc}$, which suggests that these AGNs contribute to the LG motion from much deeper distances than the IRAS or the EMSS samples. This can be explained as being due to the large redshifts of the objects in this sample. Also the amplitude at the saturation point, is found to be $\sim 617 \pm 8 \text{ km/sec}$, from which we obtain $b_{654 \text{ quasars}} \Omega_o^{-0.6} = 1.02 \pm 0.01$, which suggests that these AGNs are less clustered than the IRAS 1.2 Jy galaxies, for which $b_{IRAS} \Omega_o^{-0.6} = 1.9 \pm 0.09$.

Finally, for a further investigations, we have plotted the dipole growth curves for this sample and a sample of 178 IRAS 1.2Jy galaxies selected with the same selection function, as shown in figure 7.

Note that in these, we have assumed the bias parameter of 1.0 for both curves. This has created some overlapping between the two curves, suggesting a similar degree of clustering for both samples.

6 THE ANGULAR AND SPATIAL CORRELATION FUNCTIONS

The cross-correlation function $\xi_{ab}(r)$, between population 'a' and 'b', is defined in terms of the joint probability δP that a population 'a' object is in an infinitesimal volume element δV_a and a population 'b' in δV_b separated from δV_a and δV_b by r_{ab} :

$$\delta P = \langle n_a \rangle \langle n_b \rangle [1 + \xi_{ab}(r_{ab})] \delta V_a \delta V_b \quad (13)$$

where $\langle n_a \rangle$ and $\langle n_b \rangle$ are the mean number densities of population 'a' and 'b' respectively.

If galaxies were distributed randomly in the universe, $\xi(r)$ would be zero. If there is any distance scale over which objects tend to cluster, $\xi(r) > 0$, and if there is a scale at which the objects avoid each other (anti-clustering), $\xi(r)$ is negative within that scale. $\xi(r)$ is calculated as:

$$\xi(r) = \frac{N_{DD}(r)}{N_{DR}(r)} - \frac{n_R}{n_D} \quad (14)$$

where N_{DD} and N_{DR} refer to the number of data-data and data-random pairs, respectively; n_D and n_R refer to the mean densities of the real and random catalogues.

Note that for the analysis of the spatial correlation function, the population of the random sample is chosen to be at least 50 times more than the real sample. This random sample is selected so as to have the same selection function (ie. the same redshift distribution) as the real sample.

This function has been calculated for galaxies (Davis & Peebles, 1983; Fisher et al., 1994; etc.), clusters of galaxies (Bahcall et al., 1984) and QSOs (Shanks et al., 1987).

Note that the errors are calculated as the weighted Poissonian:

$$\delta \xi(r) \sim \sqrt{\frac{1 + \xi(r)}{N_{DR}}} \sim \frac{\sqrt{N_{DD}}}{N_{DR}} \quad (15)$$

A common feature of the spatial correlation functions, is that they can be approximated by a power law model (on small scales, $r < 10 h^{-1} \text{Mpc}$, where the galaxy distribution is characterized by strong nonlinear clustering) of the form:

$$\xi(r) = (r/r_o)^{-\gamma} \quad (16)$$

where r_o and γ are the correlation length and the power law index respectively. For galaxies, r_o is of the order $5.4 h^{-1} \text{Mpc}$ (Davis & Peebles, 1983) with $\gamma \sim 1.7 - 1.8$. This correlation length has been found to increase as the scale of the system increases (ie. a larger value of r_o is found for rich clusters and even a larger value is found for superclusters). Bahcall & Soneira (1983) found $r_o \sim 25 h^{-1} \text{Mpc}$ and $\gamma \sim 1.7$ for Abell clusters.

To find the best power law fit, we have used the method of χ^2 minimisation. and the errors on each parameter correspond to $\delta \chi^2 = 1$. Note that this method is valid only if the errors of the correlation function at a fixed separation are Gaussian distributed and if the values at different separations are uncorrelated. The power law model is usually fitted to the data for $r \leq 20 h^{-1} \text{Mpc}$ and since these separations are typically much smaller than the size of the sample, the central limit theorem ensures that the distribution of errors will be Gaussian.

According to the linear biasing theory (Kaiser, 1984), the two point correlation function between populations 'a' and 'b' can be approximated by:

$$\xi_{ab}(r) = b_a b_b \xi_m(r) \quad (17)$$

where b_a and b_b are the bias parameters (ie. the contrast enhancement factor of the distribution of tracers compared to the underlying mass distribution) for populations 'a' and 'b' respectively and $\xi_m(r)$ is the correlation function of the underlying mass density.

b is defined as:

$$b = \frac{(\frac{\delta\rho}{\rho})_{tracer}}{(\frac{\delta\rho}{\rho})_{mass}} \quad (18)$$

Calculating the correlation function of various tracers indicates the relative bias parameters of these tracers (Lahav, Nemiross et al., 1990). Also, comparing a cross-correlation function ($\xi_{IX}(r)$) with an auto-correlation function ($\xi_{II}(r)$), gives extra relative biasing between two types of mass tracers:

$$\frac{\xi_{IX}(r)}{\xi_{II}(r)} = \frac{b_X}{b_I} \quad (19)$$

Having described the calculation of the spatial correlation function, let us now have a brief review of the angular correlation function. The angular correlation function can be expressed in terms of probability in a similar way as the spatial correlation function. If one considers two differential elements of solid angle on the sky, $d\Omega_1$ and $d\Omega_2$, then the joint probability, dP , that galaxies will occupy the two elements with an angular separation of θ can be written as:

$$dP = n^2(1 + w(\theta))d\Omega_1 d\Omega_2 \quad (20)$$

where n is the mean surface density of galaxies. Note that a random (Poisson) distribution of galaxies yields $w(\theta) = 0$ for all θ . Also:

$$w = \frac{N_{DD}}{N_{RR}} - 1 \quad (21)$$

or:

$$w = \frac{N_{DD}}{N_{DR}} - 1 \quad (22)$$

Again, the errors are calculated as Poissonian errors. Finally, $w(\theta)$ can be approximated by a power law of the form:

$$w(\theta) = A\theta^{-\delta} \quad (23)$$

As before the best fit, can be found using the methods of χ^2 minimisation, and the errors on each parameter correspond to $\delta\chi^2=1$

7 THE RESULTS OF THE ANGULAR AND SPATIAL CORRELATION FUNCTION CALCULATIONS

The results of the various angular and spatial auto and cross correlation functions are shown in figures 8-15.

The best power law fit to all the data analysed in this work are shown in solid lines. For further comparisons, we have also plotted power law fits from previous work. For angular correlation functions, these are: the fit found by Woods et al. (1997), studying the angular auto-correlation function for faint optical galaxies in high galactic latitude fields: $w(\theta) = 0.508 \theta^{-0.8}$ (shown as the dotted line); and the fit by Lidman et al. (1996), studying the two point angular auto-correlation function for a sample of optical galaxies selected

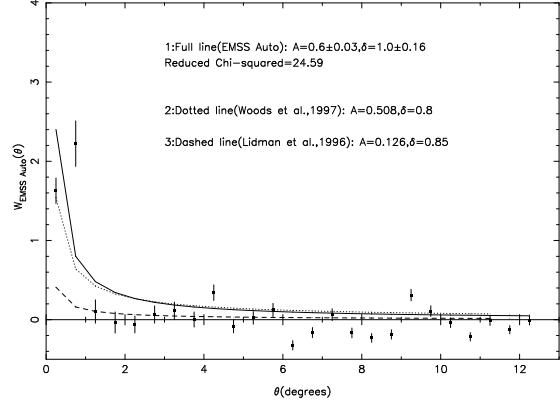


Figure 8. The EMSS AGNs Angular Auto-Correlation Function

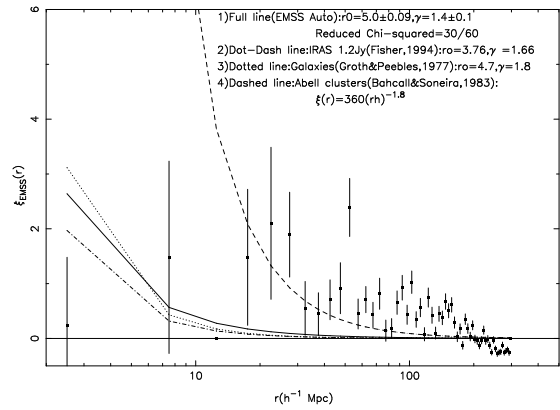


Figure 9. The EMSS AGNs Spatial Auto-Correlation Function

from two large format CCD surveys: $w(\theta) = 0.126 \theta^{-0.85}$ (shown as the dashed line).

For the spatial correlation functions, these are: The power law fitted by Fisher et al. (1994), calculating the spatial auto-correlation function for the IRAS 1.2 Jy galaxies (shown as the dot-dash curve): $\xi(r) = (r/3.76)^{-1.66}$; a general fit found for the galaxy auto-correlation (Groth & Peebles, 1977), shown by the dotted line: $\xi(r) = (r/4.7)^{-1.8}$; and finally the fit found for the Abell clusters auto-correlation (Bahcall & Soneira, 1983), presented as the dashed line: $\xi(r) = 360(rh)^{-1.8}$.

It is important to note that there is a linear dependence between the scale of the system and the correlation length (ie. the scale of clustering). r_o is found to be $\sim 5h^{-1} Mpc$ for galaxies and $\sim 25h^{-1} Mpc$ for Abell clusters.

Furthermore, we have compared the average amplitudes for various samples for different angular and distance separations, as shown in Tables 1-4.

Note that from all these comparisons, it appears that AGN / quasar samples are less clustered than the galaxy samples, and this is consistent with the results of the dipole analysis. Note that AGNs are rare distance objects, and this puts limits to the accuracy of the correlation signals at small scales. In the spatial correlation functions, there are relatively large

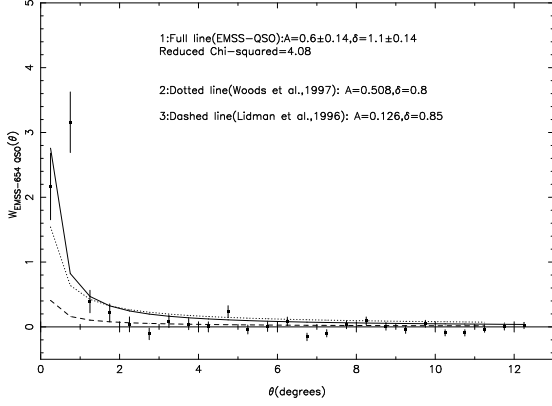


Figure 10. The EMSS AGNs-654 QSO Angular Cross-Correlation Function

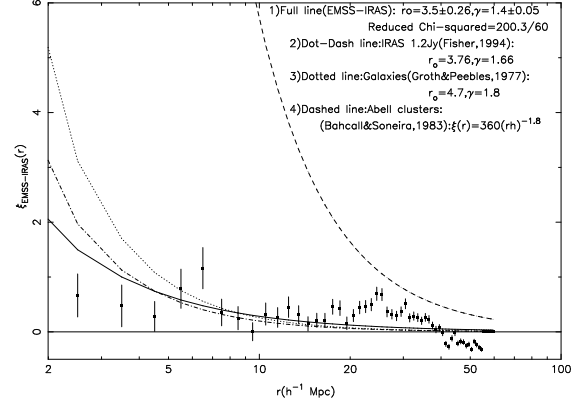


Figure 13. The EMSS AGNs-IRAS 1.2 Jy galaxies Spatial Cross-Correlation Function

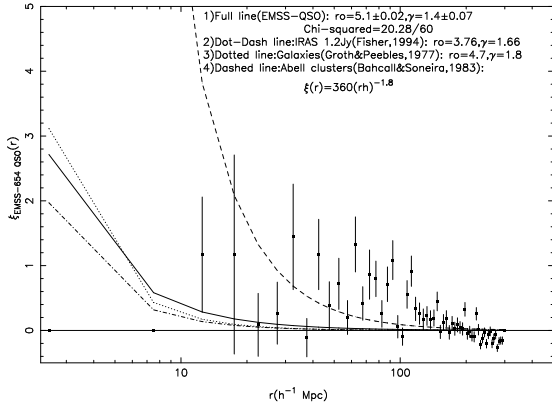


Figure 11. The EMSS AGNs-654 QSO Spatial Cross-Correlation Function

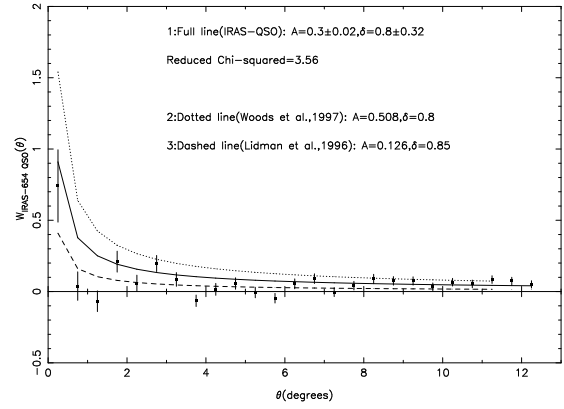


Figure 14. The IRAS 1.2 Jy sample-654 QSO Angular Cross-Correlation Function

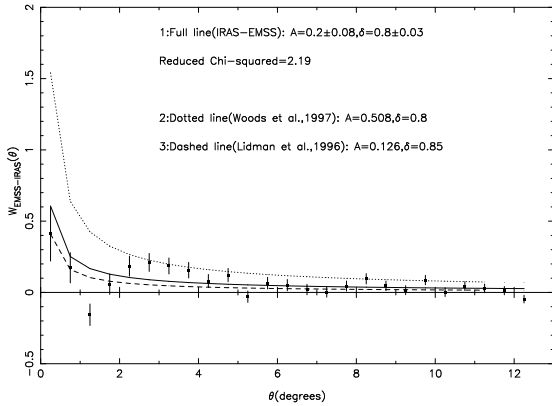


Figure 12. The EMSS AGNs-IRAS 1.2 Jy galaxies Angular Cross-Correlation Function

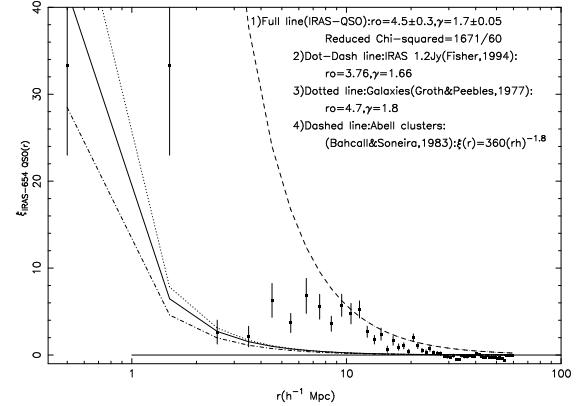


Figure 15. The IRAS 1.2 Jy sample-654 QSO Spatial Cross-Correlation Function

error bars at small scales ($r < 10h^{-1}Mpc$) and the data is consistent with zero.

Finally, the relative bias parameters between various samples (at $r = 12.5 h^{-1} Mpc$) are found to be:

$$b_{IRAS}/b_{654quasar} = 3.6 \pm 2.7 \quad (24)$$

$$b_{IRAS}/b_{EMSS} = 8.5 \pm 6.4 \quad (25)$$

$$b_{654quasars}/b_{EMSS} = 2.4 \pm 0.2 \quad (26)$$

which again suggests that AGNs / quasars are less clustered than the IRAS galaxies.

8 DISCUSSION

Having obtained different bias parameters for different samples of AGNs, using the dipole moment and the standard methods of spatial and angular correlation functions, let us now briefly discuss the calculation of the spatial correlation function for a fractal.

Analysis of galaxy and cluster correlations based on the concepts and methods of modern statistical Physics, led to the suggestion that galaxy correlations are fractals and not homogeneous to the limits of the available catalogs (Pietronero, 1987; Coleman et al., 1992).

According to these analysis, galaxy structures are highly irregular and self-similar: all the available data are consistent with each other and show fractal correlations (with dimensions, $D \sim 2$) up to the deepest scales probed so far (eg. $1000 h^{-1}Mpc$). If galaxy distribution becomes really homogeneous at a scale λ_o within the sample in question (ie. if $\lambda_o \ll R_{eff}$, where R_{eff} is the effective depth of the sample), then one has $r_o = \lambda_o 2^{1/(D-3)}$. For a fractal of dimension $D \sim 2$, therefore: $r_o \sim \lambda_o/2$. If on the other hand, the fractal correlations extend up to the sample limits, then the resulting value of r_o has nothing to do with the real properties of the galaxy distribution, but it is fixed by the size of the sample.

The expression of $\xi(r)$ in the case of fractal distribution is:

$$\xi(r) = \frac{3-\gamma}{3} \left(\frac{r}{R_s}\right)^{-\gamma} - 1 \quad (27)$$

where R_s is the depth of the spherical volume where one computes the average density.

The so-called correlation length, r_o , is a linear function of the sample size, R_s ,

$$r_o = \left(\frac{3-\gamma}{6}\right)^{1/\gamma} R_s \quad (28)$$

and hence it is a spurious quantity without physical meaning, but it is simply related to the sample size. Note that according to the above equation, there is a linear dependence between the *scale/size* of the system and the correlation length, and this is consistent with the results from the standard power law model of the correlation function. In other words, as the size of the sample increases (*ie.* R_s), the value of the correlation length increases (cf. $r_o \sim 5h^{-1}Mpc$ for galaxies, and $r_o \sim 25h^{-1}Mpc$ for Abell clusters).

Finally note that if the distribution is fractal, even the dipole moment is affected, and its value depends on even very distant objects, although weighted by $1/r^2$.

9 SUMMARY OF CONCLUSIONS

From the above analysis (the dipole moment and the correlation function), it appears that the EMSS AGNs are less clustered than the sample of 654 ROSAT detected quasars which itself is less clustered than the IRAS galaxies. This was numerically shown by the values of the bias parameters.

From the dipole analysis, we deduced the values of $R_{conv} \sim 300 - 400h^{-1}Mpc$ for the EMSS AGNs and $\sim 450 - 500h^{-1}Mpc$ for the quasar sample, from which it appears that these AGNs / quasars have a gravitational effect on the LG motion from much deeper distances than IRAS galaxies ($R_{conv} \sim 40 - 100h^{-1}Mpc$) and Abell clusters ($R_{conv} \sim 160h^{-1}Mpc$). Also the amplitudes of the dipole growth curves at the saturation region are found to be 405.4 ± 103.36 km/sec for the EMSS AGNs and 617.3 ± 8.35 km/sec for the quasar sample, from which we find: $b_{EMSS}\Omega_o^{-0.6} = 0.68 \pm 0.22$ for the EMSS sample, and $b_{654quasars}\Omega_o^{-0.6} = 1.02 \pm 0.014$ for the quasar sample. Comparing the maximum amplitudes at the saturation region, suggests that the more sensitive the sample (ie. the lower the flux limit), the less clustered it is compared to the underlying mass distribution.

Assuming that $b\Omega_o^{-0.6} \sim 1$, which is supported by deep AGN samples, we conclude $\Omega_o \simeq 1$ if $b \simeq 1$. However to obtain $\Omega_o \simeq 0.3$ (Krauss, 1998), requires b significantly less than 1. From the correlation function analysis, it appears that the AGN / quasar samples are less clustered than the galaxies, which is consistent with the results of the dipole calculations. The values of the relative bias parameters were found to be: $b_{IRAS}/b_{654-quasar} = 3.61 \pm 2.7$, $b_{IRAS}/b_{EMSS} = 8.46 \pm 6.4$ and $b_{654-quasars}/b_{EMSS} = 2.35 \pm 0.2$. However the validity of these values is subject to the criticism that they are sample depth dependent.

REFERENCES

- Bahcall N., Soneira R., 1983, ApJ, 270, 20
 Bahcall N., Soneira R., 1984, ApJ, 277, 27
 Branchini E., Plionis M., 1996, ApJ, 460, 569
 Brinkmann W., Yuan W., Siebert J, et al., 1997, A&A, 319, 413
 Coleman P.& Pietronero L., 1992, Phys. Rep., 231, 311
 Davis M.& Peebles P., 1983, ApJ, 267, 465
 Fisher K., Davis M., Strauss M., 1994, MNRAS, 266, 50
 Gioia I., Maccacaro T., et al., 1990, ApJS, 72, 567
 Hudson M.J., 1993, MNRAS, 265, 72
 Kaiser, 1984, ApJ, 284, L9
 Krauss L., 1998, ApJ, 501, 461
 Lahav O., 1987, MNRAS, 225, 213
 Lahav O., Rowan-Robinson M., Lynden-Bell, et al., 1988, ApJ, 326, 19
 Lahav O., Edge A.C., Fabian A., et al., 1989, MNRAS, 238, 881
 Lahav O., Nemiroff J. et al., 1990, ApJ, 350, 119
 Lidman C., Peterson, 1996, MNRAS, 279, 1357
 Maccacaro T., Ceca R., Gioia L, et al., 1991, ApJ, 374, 117
 Miyaji T., Bolt E., 1990, ApJ, 353, L3
 Peacock J.& Nicholson D., 1991, MNRAS, 253, 307
 Peebles P., 1980, The Large structure of the Universe, Princeton University Press
 Pietronero L., 1987, Physica A, 144, 257
 Plionis M. & Kolokotronis., 1998, ApJ, 500, June 10th issue
 Rowan-Robinson M., et al., 1990, MNRAS, 247, 1
 Scaramella R., et al., 1991, ApJ, 376, L1

θ	$\langle W_{EMSS} \rangle$	$\langle W_{EMSS-654QSO(Cross)} \rangle$	$\langle W_{IRAS} \rangle$	$\langle W_{Woods} \rangle$	$\langle W_{Lidman} \rangle$
$1.5^\circ < \theta < 5^\circ$	0.05 ± 0.07	0.074 ± 0.09	0.14 ± 0.07	0.21	0.05

Table 1. Comparing the average amplitude of the X-ray AGNs Angular Correlation functions with those of IR/Optical galaxy Auto-Correlation functions

θ	$\langle W_{EMSS-IRAS(Cross)} \rangle$	$\langle W_{IRAS-654QSO(Cross)} \rangle$	$\langle W_{IRAS} \rangle$	$\langle W_{Woods} \rangle$	$\langle W_{Lidman} \rangle$
$\theta < 1.5^\circ$	0.14 ± 0.12	0.23 ± 0.13	0.25 ± 0.11	0.79	0.23
$1.5^\circ < \theta < 5^\circ$	0.14 ± 0.06	0.05 ± 0.07	0.14 ± 0.07	0.21	0.05

Table 2. Comparing the average amplitude of the AGNs-galaxies Angular Cross-Correlation functions with those of IR/Optical galaxy Auto-Correlation functions

Schmidt M.& Green R., 1986, ApJ, 305, 68
 Strauss M.A., Yahil A., Davis, et al., 1992, ApJ, 397, 395
 Stocke et al., 1991, ApJS, 76, 813
 Page M. et al., 1996, MNRAS, 281, 579
 Plionis & Valdernini, 1991, MNRAS, 249, 46
 Voges W. et al., 1992, In: Proc.of the ISY Conference "Space Science",
 ESA ISY-3, ESA Publications, P.223
 Voges W., et al., 1995, ROSAT NEWS No.32
 Woods D., Fahlman G., 1997, ApJ, 490, 11
 Yahil A., Walker D., Rowan-Robinson M., 1986, ApJ, 301, L1

$r(h^{-1}Mpc)$	$\langle \xi_{EMSS} \rangle$	$\langle \xi_{EMSS-654QSO(Cross)} \rangle$	$\langle \xi_{IRAS} \rangle$	$\langle \xi_{galaxies} \rangle$	$\langle \xi_{Abellclusters} \rangle$
$r < 10$	0.86 ± 1.49	no signals!	1.15	1.78	39.4
$10 < r < 20$	0.81 ± 0.6	1.84 ± 1.2	0.11	0.13	2.96
$20 < r < 50$	7.4 ± 0.64	6.9 ± 0.5	0.03	0.03	0.7

Table 3. Comparing the average amplitude of the X-ray AGNs Spatial Correlation functions with those of IR/Optical galaxy Auto-Correlation functions

$r(h^{-1}Mpc)$	$\langle \xi_{EMSS-IRAS(Cross)} \rangle$	$\langle \xi_{IRAS-654QSO(Cross)} \rangle$	$\langle \xi_{IRAS} \rangle$	$\langle \xi_{galaxies} \rangle$	$\langle \xi_{Abellclusters} \rangle$
$r < 10$	0.58 ± 0.34	10.3 ± 3.2	3.86	7.25	161.1
$10 < r < 20$	0.29 ± 0.15	2.15 ± 0.58	0.1	0.13	3.03

Table 4. Comparing the average amplitude of the AGNs-galaxies Spatial Cross-Correlation functions with those of IR/Optical galaxy Auto-Correlation functions